Spectral Global Intrinsic Symmetry Invariant Functions

Hui Wang*
Shijiazhuang Tiedao University

Patricio Simari†
The Catholic University of America

Zhixun Su‡
Dalian University of Technology

Hao Zhang§
Simon Fraser University

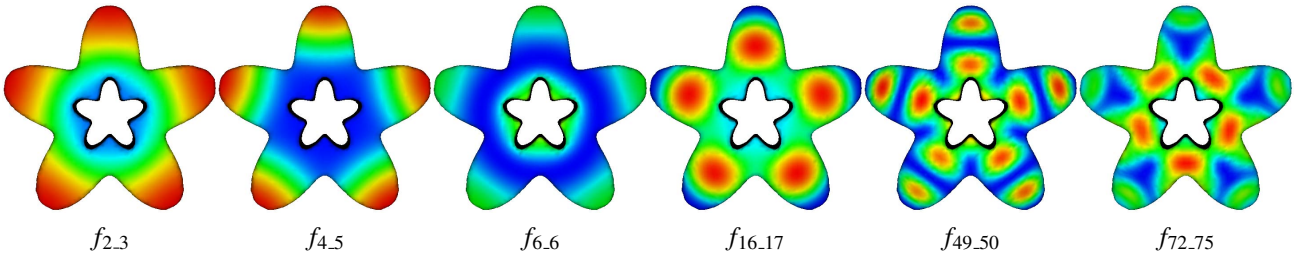

Figure 1: Spectral Global Intrinsic Symmetry Invariant Functions (GISIFs) computed on a five-point star with rotational symmetries; f_{i_j} denotes a GISIF computed using eigenfunctions of the Laplace-Beltrami operator corresponding to repeated eigenvalues i through j (see Eq. 7).

Abstract

We introduce spectral Global Intrinsic Symmetry Invariant Functions (GISIFs), a class of GISIFs obtained via eigendecomposition of the Laplace-Beltrami operator on compact Riemannian manifolds, and provide associated theoretical analysis. We also discretize the spectral GISIFs for 2D manifolds approximated either by triangle meshes or point clouds. In contrast to GISIFs obtained from geodesic distances, our spectral GISIFs are robust to topological changes. Additionally, for symmetry analysis, our spectral GISIFs represent a more expressive and versatile class of functions than the classical Heat Kernel Signatures (HKSs) and Wave Kernel Signatures (WKSs). Finally, using our defined GISIFs on 2D manifolds, we propose a class of symmetry-factored embeddings and distances and apply them to the computation of symmetry orbits and symmetry-aware segmentations.

1 Introduction

Symmetry is ubiquitous in both naturally-occurring and human-manufactured shapes. Thus, detecting symmetries and finding symmetry invariants represents an important research problem in computer graphics with many applications [12], especially for global intrinsic symmetries [6, 15, 18].

Global Intrinsic Symmetry Invariant Functions (GISIFs), which are functions defined on a manifold invariant under all global intrinsic symmetries, have received much attention in the context of shape analysis [6, 9, 14]. For example, the critical points of the GISIFs obtained via geodesic distances form symmetry invariant point sets for the generation of candidate Möbius transformations [6]. GISIFs such as the classical Heat Kernel Signature (HKS) [22] and Wave Kernel Signature (WKS) [1] are also used as symmetry invariant descriptors for shape correspondence [14].

In this paper, we propose a new class of GISIFs over compact Riemannian manifolds via spectral methods, where each eigenvalue of the Laplace-Beltrami operator, either repeated or non-repeated, corresponds to a GISIF. Our spectral GISIFs have advantages over those which have been previously-proposed. First, spectral GISIFs demonstrate a robustness to topological changes, a property not found in GISIFs based on geodesic distances. Furthermore, the HKS and WKS are linear combinations of our spectral GISIFs. The key difference between the HKS, WKS, and our spectral GISIF is that the HKS and WKS combine all eigenfunctions of the Laplace-Beltrami operator, while we define a spectral GISIF for each eigenvalue, either repeated or non-repeated, using its corresponding eigenfunctions. As such, the new GISIFs represent a broader and more versatile class of functions.

We generate symmetry-factored embeddings from spectral GISIFs and apply them to compute symmetry orbits and symmetry-aware segmentations. In contrast to previous works, which use only non-repeated eigenvalues [9], we use eigenfunctions of the Laplace-Beltrami operator corresponding to both repeated and non-repeated eigenvalues. We will show this allows our embeddings to better capture rotational symmetries, not only reflectional symmetries.

2 Related Work

Global Intrinsic Symmetry Invariant Functions. Symmetry detection and analysis are fundamental problems in computer graphics, image processing, and computer vision [3, 12]. Recent works in computer graphics focus mainly on analyzing global and partial intrinsic symmetries and on leveraging symmetries in shape processing and analysis [6, 11, 15, 25]. For an in-depth survey of such methods and applications, we refer the interested reader to a recent state-of-the-art survey [12]. In this section, we will focus on overviewing previous work in the area of GISIFs.

To the best of our knowledge, Kim et al. are the first to propose a class of GISIFs based on geodesic distances, and they use the critical points of these GISIFs as sampling points for the generation of candidate Möbius transformations [6]. In this paper, we introduce a new class of GISIFs based on the spectral method. Compared to GISIFs obtained with geodesic distances, our spectral GISIFs are more robust to topological changes, as illustrated in Figure 8.

Lipman et al. [9] introduce the concept of a symmetry-invariant function space, and use a symmetry correspondence matrix to symmetrize functions on shapes. However, for their global intrinsic symmetry dissimilarity measure, they only use those eigenfunctions which correspond to non-repeated eigenvalues of the Laplace-Beltrami operator, making it difficult to handle shapes with rota-

*e-mail:wangh@stdu.edu.cn; this research work was initially conducted when the first author visited Simon Fraser University.
†e-mail:mail:simari@cua.edu
‡e-mail:zxsu@dlut.edu.cn
§e-mail:haoz@cs.sfu.ca

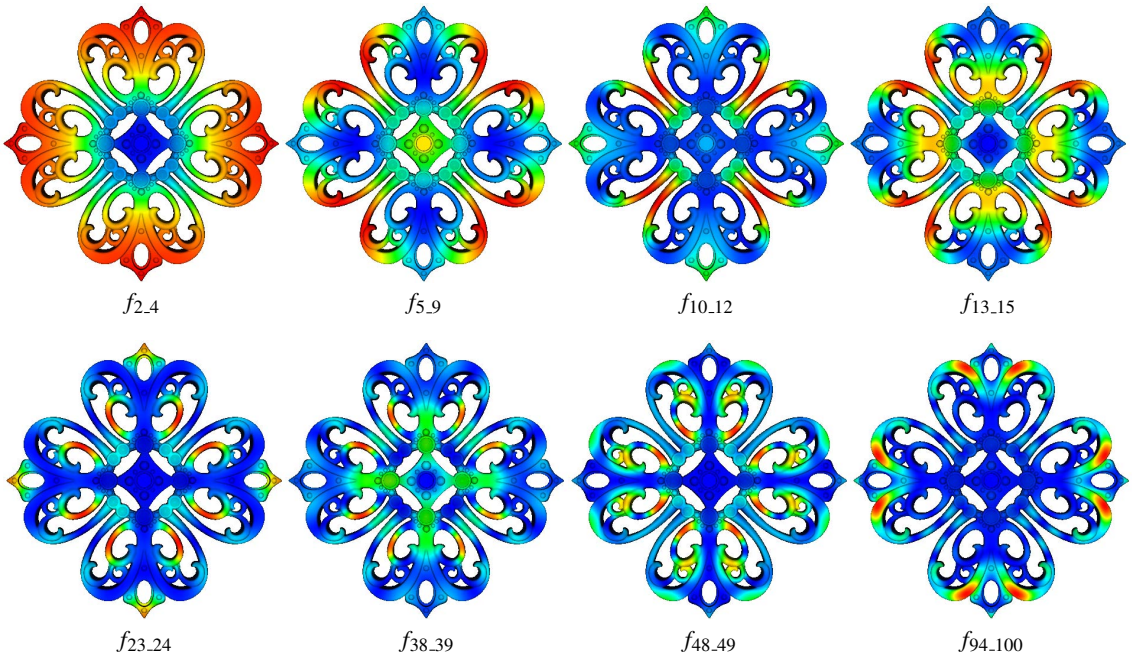

Figure 2: Spectral GISIFs on a filigree triangle mesh.

tional symmetries. In contrast, our spectral GISIFs utilize eigenfunctions corresponding to both repeated and non-repeated eigenvalues, allowing better capture of such symmetries.

The classical Heat Kernel Signature (HKS) [22] and Wave Kernel Signature (WKS) [1] are also GISIFs and can be used as symmetry invariant descriptors for shape correspondence [14]. The Auto Diffusion Function (ADF), in turn, is used for skeletonization and segmentation [5]. Interestingly, all three of these signatures are linear combinations of our spectral GISIFs so our approach can be viewed as a generalization of these and other such global symmetry invariant functions.

Spectral methods using Laplace-Beltrami Operator. The Laplace-Beltrami operator and its spectra are widely used in computer graphics for shape processing and analysis [7, 8, 23], with applications including shape retrieval [19], intrinsic embedding [21], global intrinsic symmetry detection [15], heat kernel signature [22], and shape correspondence [13].

In this paper, we propose spectral GISIFs, a class of GISIFs based on the spectra of the Laplace-Beltrami operator. Our work is inspired by spectral global intrinsic symmetry detection [15], which uses only the eigenfunctions corresponding to non-repeated eigenvalues of the Laplace-Beltrami operator. However, if a compact manifold has a symmetry T such that $T^2 \neq I$, then the eigenvalues of the Laplace-Beltrami operator of the manifold must have repeated eigenvalues, as pointed out in [16]. Here, we take a first step toward using the eigenfunctions corresponding to the repeated eigenvalues of the Laplace-Beltrami for symmetry analysis.

3 Spectral GISIFs on Riemannian Manifolds

In this section, we define global intrinsic symmetry and GISIFs and then construct a class of GISIFs over compact Riemannian manifolds via the eigendecomposition of the Laplace-Beltrami operator.

3.1 Global Intrinsic Symmetry

A global intrinsic symmetry on a particular manifold is a geodesic distance-preserving self-homeomorphism [15, 18].

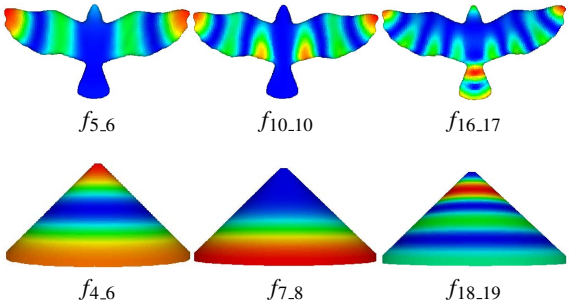

Figure 3: Spectral GISIFs on a bird and cone point cloud.

Definition 1: A self-homeomorphism $T : M \to M$ that preserves all geodesic distances on manifold M is called a global intrinsic symmetry; i.e., it holds that

$$g(\mathbf{p},\mathbf{q}) = g(T(\mathbf{p}),T(\mathbf{q})), \tag{1}$$

for all $\mathbf{p},\mathbf{q} \in M$, where $g(\mathbf{p},\mathbf{q})$ is the geodesic distance from $\mathbf{p}$ to $\mathbf{q}$.

The set of all global intrinsic symmetries on the manifold M forms a group $G(M)$ called the symmetry group with composition as the group operation. Obviously the identity mapping I on the manifold M is an element of the group $G(M)$.

3.2 Global Intrinsic Symmetry Invariant Function

Definition 2: Suppose $f : M \to \mathbb{R}$ is a function defined on the manifold M. If every global intrinsic symmetry T on M satisfies $f \circ T = f$, that is

$$f \circ T(\mathbf{p}) = f(T(\mathbf{p})) = f(\mathbf{p}), \tag{2}$$

for all $\mathbf{p} \in M$, then f is a global intrinsic symmetry invariant function. Note that this definition is the same as that of Kim et al. [6]. The following useful propositions can be easily obtained:

1. Constant functions $f(\mathbf{p}) = c$, for all $\mathbf{p}$ in manifold M are GISIFs.

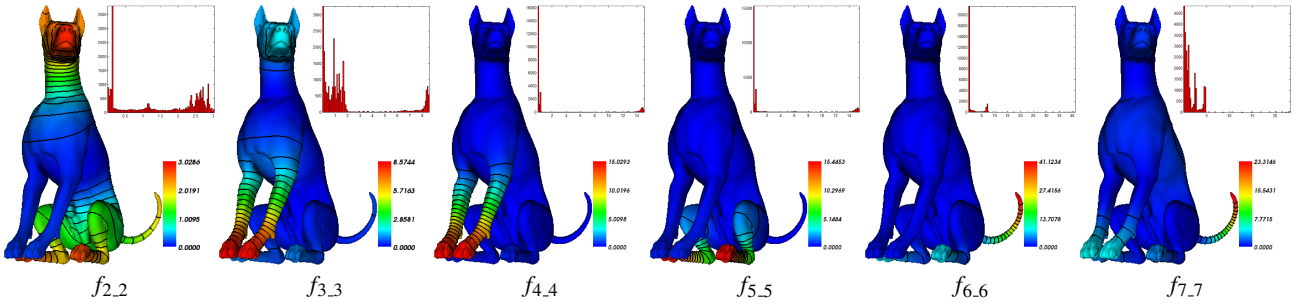

Figure 4: Level sets and histograms of our spectral GISIFs on a dog model. The large blue areas without contours along with the histograms of each field (above), which show a large fraction of values to be near-zero, illustrate the sparsity of the fields.

2. If f is a GISIF on manifold M, then $c*f$ (where c is a constant) is also a GISIF on M.

3. If functions f and g are GISIFs on manifold M, then $f+g$, $f-g$, $f*g$, $f/g(g\neq 0)$ are GISIFs on M.

Based on the above propositions, all of the GISIFs defined on M form a linear space $F^+(M)$ called the global intrinsic symmetry invariant function space, which is a subspace of the functional space $F(M)$ on M. Further, if $G:(F(M),F(M),\ldots,F(M))\rightarrow F(M)$ is a linear operator, then $G(F^+(M),F^+(M),\ldots,F^+(M))\subseteq F^+(M)$.

3.3 Spectral GISIFs via the Laplace-Beltrami Operator

We propose a new class of GISIFs based on the eigendecomposition of the Laplace-Beltrami operator on compact Riemannian manifolds without boundaries. Each GISIF corresponds to an eigenvalue, repeated or non-repeated, of the Laplace-Beltrami operator.

Theorem 1: Suppose M is a compact Riemannian manifold without boundary, λ_i is an eigenvalue of the Laplace-Beltrami operator Δ on M with a k-dimensional eigenfunction space. If $\phi_{i1},\phi_{i2},\cdots,\phi_{ik}$ is an orthogonal basis of the corresponding eigenfunction space of λ_i, then the following function

$$f(\mathbf{p})=\sum_{j=1}^{k}\phi_{ij}^2(\mathbf{p}), \tag{3}$$

for all $\mathbf{p}\in M$, is a GISIF on M.

Proof: $\phi_{i1},\phi_{i2},\cdots,\phi_{ik}$ is an orthogonal basis of the k-dimensional eigenfunction space of eigenvalue λ_i of Δ on M. Then

$$<\phi_{ij},\phi_{il}>=\delta_{jl}=\begin{cases}1, & j=l\\ 0, & j\neq l\end{cases}\quad j,l\in\{1,2,\cdots,k\}.$$

For every global intrinsic symmetry $T:M\rightarrow M$, $\phi_{i1}\circ T,\phi_{i2}\circ T,\cdots,\phi_{ik}\circ T$ are also eigenfunctions corresponding to the eigenvalue λ_i [15, 20], satisfying the following equation

$$<\phi_{ij}\circ T,\phi_{il}\circ T>=\delta_{jl}=\begin{cases}1, & j=l\\ 0, & j\neq l\end{cases}\quad j,l\in\{1,2,\cdots,k\}.$$

That is, $\phi_{i1}\circ T,\phi_{i2}\circ T,\cdots,\phi_{ik}\circ T$ is also an orthogonal basis of the corresponding eigenfunction space of the eigenvalue λ_i. Then, there exists a k-dimensional orthogonal matrix $\mathbf{A}$ ($\mathbf{A}\mathbf{A}^T=\mathbf{A}^T\mathbf{A}=\mathbf{I}$, where $\mathbf{I}$ is the k-dimensional identity matrix) such that:

$$\begin{aligned}&(\phi_{i1}(T(\mathbf{p})),\phi_{i2}(T(\mathbf{p})),\cdots,\phi_{ik}(T(\mathbf{p})))\\&=(\phi_{i1}(\mathbf{p}),\phi_{i2}(\mathbf{p}),\cdots,\phi_{ik}(\mathbf{p}))*\mathbf{A},\end{aligned}$$

for all $\mathbf{p}\in M$. So we have

$$\begin{aligned}&f\circ T(\mathbf{p})=f(T(\mathbf{p}))=\sum_{j=1}^{k}\phi_{ij}^2(T(\mathbf{p}))\\&=(\phi_{i1}(T(\mathbf{p})),\phi_{i2}(T(\mathbf{p})),\cdots,\phi_{ik}(T(\mathbf{p})))*\\&(\phi_{i1}(T(\mathbf{p})),\phi_{i2}(T(\mathbf{p})),\cdots,\phi_{ik}(T(\mathbf{p})))^T\\&=(\phi_{i1}(\mathbf{p}),\phi_{i2}(\mathbf{p}),\cdots,\phi_{ik}(\mathbf{p}))*\mathbf{A}*\mathbf{A}^T*(\phi_{i1}(\mathbf{p}),\phi_{i2}(\mathbf{p}),\cdots,\phi_{ik}(\mathbf{p}))^T\\&=(\phi_{i1}(\mathbf{p}),\phi_{i2}(\mathbf{p}),\cdots,\phi_{ik}(\mathbf{p}))*\mathbf{I}*(\phi_{i1}(\mathbf{p}),\phi_{i2}(\mathbf{p}),\cdots,\phi_{ik}(\mathbf{p}))^T\\&=(\phi_{i1}(\mathbf{p}),\phi_{i2}(\mathbf{p}),\cdots,\phi_{ik}(\mathbf{p}))*(\phi_{i1}(\mathbf{p}),\phi_{i2}(\mathbf{p}),\cdots,\phi_{ik}(\mathbf{p}))^T\\&=\sum_{j=1}^{k}\phi_{ij}^2(\mathbf{p})=f(\mathbf{p}).\end{aligned}$$

Therefore, the function defined in Equation (3) is a global intrinsic symmetry invariant function on M. □

4 Discretization on 2-manifolds

In this section, the spectral GISIFs proposed in the above section are discretized on 2D manifolds approximated either by triangle meshes or point clouds. We also illustrate some examples of our spectral GISIFs and show their properties and advantages.

4.1 Implementation

Discretization on Triangular Meshes. A 2D compact manifold M can be approximated by a triangle mesh $\mathrm{TRI}=(\mathbf{V},\mathbf{E},\mathbf{F})$, where $\mathbf{V}=\{\mathbf{v}_1,\mathbf{v}_2,\ldots,\mathbf{v}_n\}$ denotes the set of vertices, $\mathbf{E}=\{(i,j)\mid \mathbf{v}_i$ and $\mathbf{v}_j\in\mathbf{V}$ linked by an edge$\}$ denotes the set of edges, and $\mathbf{F}=\{(i,j,k)\mid \mathbf{v}_i,\mathbf{v}_j,\mathbf{v}_k\in\mathbf{V}$ linked by a face$\}$ denotes the set of faces. $N(i)=\{j\mid(i,j)\in\mathbf{E}\}$ is the set of vertex indices of the 1-ring neighbors of $\mathbf{v}_i$. A function $f:M\rightarrow\mathbb{R}$ on M is approximated by a piecewise-linear scalar function defined by linearly interpolating the values of f at the vertices $\mathbf{f}=(f(\mathbf{v}_1),f(\mathbf{v}_2),\ldots,f(\mathbf{v}_n))^T$ of TRI.

For the approximation of the Laplace-Beltrami operator Δ on triangle meshes, different methods have been introduced [24]. In this paper, we use the cotangent scheme originally proposed by [4, 17], where Δ is discretized as an n-dimensional Laplacian matrix $\mathbf{L}$. This matrix is represented as $\mathbf{L}=\mathbf{S}^{-1}\mathbf{M}$, where $\mathbf{S}$ is a diagonal matrix whose i-th diagonal element is the Voronoi cell area of vertex $\mathbf{v}_i$ proposed in [4], and $\mathbf{M}$ is a symmetric matrix holding the well known cotangent weights:

$$\mathbf{M}_{ij}=\begin{cases}\sum_{k\in N(i)}w_{ik}, & i=j\\ -w_{ij}, & j\in N(i)\\ 0, & otherwise\end{cases}, \tag{4}$$

where $w_{ij}=\frac{cot\alpha_{ij}+cot\beta_{ij}}{2}$, α_{ij} and β_{ij} are angles opposite edge (i,j).

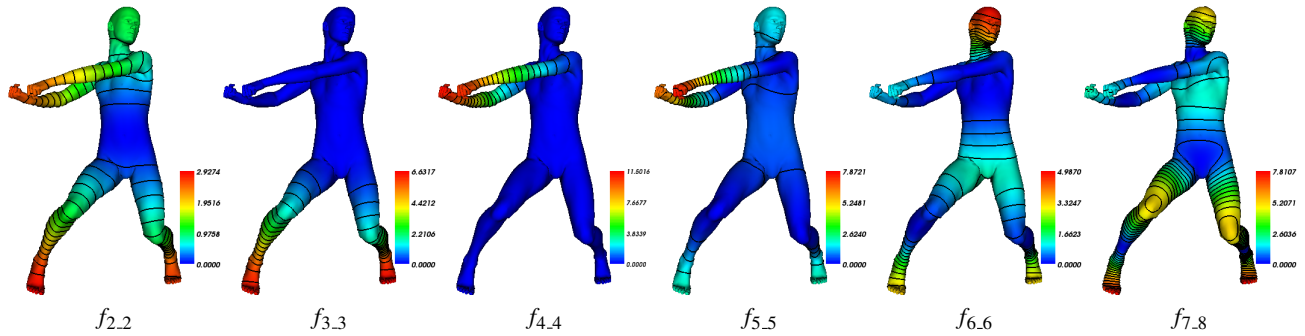

Figure 5: Level sets of our spectral GISIFs on a human model. The large blue areas without contours showing a large fraction of values to be near-zero illustrate the sparsity of the fields.

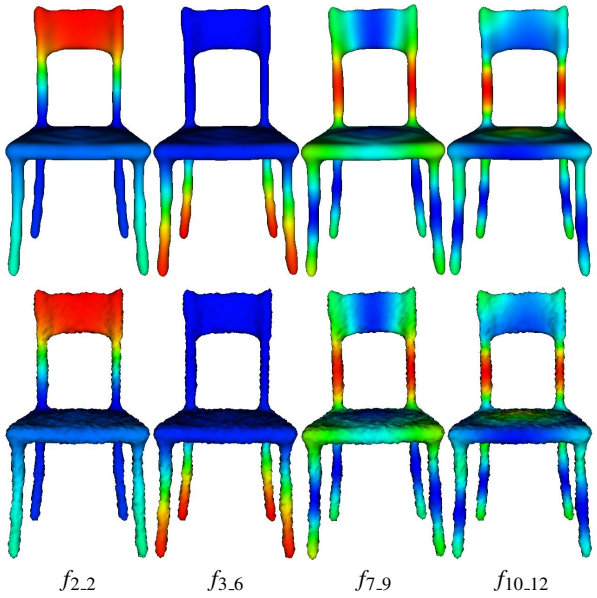

Figure 6: The spectral GISIFs corresponding to the smallest eigenvalues are insensitive to noise. **Top:** results on the original mesh. **Bottom:** results on the mesh corrupted with Gaussian noise with variance set to 20% of the mean edge length. Note the visual similarity despite the noise.

The eigendecomposition $\Delta f = \lambda f$ of the Laplace-Beltrami operator can be discretized as the following problem,

$$\mathbf{Lf} = \lambda \mathbf{f}, \tag{5}$$

where $\mathbf{f} = (f(\mathbf{v}_1), f(\mathbf{v}_2), \ldots, f(\mathbf{v}_n))^T$ is a vector with elements sampling the values of f at the vertices. Equation (5) can be converted into a generalized eigenvalue problem, i.e.,

$$\mathbf{Mf} = \lambda \mathbf{Sf}. \tag{6}$$

Discretization on Point Clouds. A 2D compact manifold M can also be approximated by a point cloud P, where $\{\mathbf{p}_1, \mathbf{p}_2, \ldots, \mathbf{p}_n\}$ denotes the set of points in P. A function $f : M \to \mathbb{R}$ on M is approximated by a vector $\mathbf{f} = (f(\mathbf{p}_1), f(\mathbf{p}_2), \ldots, f(\mathbf{p}_n))^T$, which samples the values of f at the vertices. There are several approaches for computing the discrete Laplace-Beltrami operator on point clouds [2, 10, 26]. Although any of these methods could be used to compute our spectral GISIFs, we use the approach proposed in [10], where the Laplace-Beltrami operator is discretized as an $n \times n$ matrix $\mathbf{L} = \mathbf{GD}$, where $\mathbf{D}$ is a diagonal matrix and $\mathbf{G}$ is a symmetric matrix. The eigendecomposition $\mathbf{Lf} = \lambda \mathbf{f}$ can also be converted into a generalized eigenvalue problem (see Section 3.2.1 in [10]).

Computation of GISIFs. In our experiments, we use MATLAB's *eigs* solver to solve the generalized eigenvalue problems on both triangle meshes and point clouds. Let us denote the eigenvalues as $\lambda_1 \leq \lambda_2 \leq \ldots \leq \lambda_n$, and their corresponding eigenvectors as $\phi_1, \phi_2, \ldots, \phi_n$. While the computed eigenvalues are, in practice, seldom exactly equal, if the differences ε between λ_i, λ_{i+1}, ..., and λ_{i+k} are sufficiently small, we regard λ_i as a repeated eigenvalue, and the GISIF f_{i_i+k} corresponding to λ_i is defined as follows

$$f_{i\_i+k}(\mathbf{v}_l) = \sum_{j=0}^{k} \phi_{i+j}^2(l), l \in \{1, 2, \ldots, n\}. \tag{7}$$

In practice, ε is dependent on the input model, and automatically choosing this threshold for all models is difficult.

4.2 Spectral GISIF Results

All scalar functions on triangle meshes and point clouds in this paper are displayed using colormaps where the low, middle, and high function values are represented as blue, green, and red respectively.

We illustrate several spectral GISIFs across different triangle meshes (Figures 1 and 2) and point clouds (Figure 3). It can be seen that the spectral GISIFs corresponding to the first smallest eigenvalues are smoothest. This is because the eigenfunctions of the first smallest eigenvalues represent the lowest frequencies. For most applications, the spectral GISIFs corresponding to the first 100 smallest eigenvalues, either repeated or non-repeated, of the Laplace-Beltrami operator suffice.

Sparsity property. In practice, we empirically find that most of our spectral GISIFs are sparse; that is, most of the function values of a particular GISIF are close to zero. Figures 4 and 5 show the level sets of our spectral GISIFs on two mesh models, and Figures 4 also displays their histograms. It can be seen that the sparsity property holds for most of the GISIFs in these two figures.

Robustness to noise. Figure 6 illustrates that the spectral GISIFs corresponding to the first smallest eigenvalues are robust to noise. This is because the noise lies in the higher frequencies, which do not affect the GISIFs built from the lower frequencies.

Comparisons with the Heat Kernel Signature. As previously noted, the classical Heat Kernel Signature (HKS) [22] and Wave Kernel Signature (WKS) [1] are widely used in shape analysis, where HKS is defined with a time scale

$$HKS_t(\mathbf{v}_i) = \sum_{j=1}^{n} e^{-\lambda_j t} \phi_j^2(i), i \in \{1, 2, \ldots, n\}. \tag{8}$$

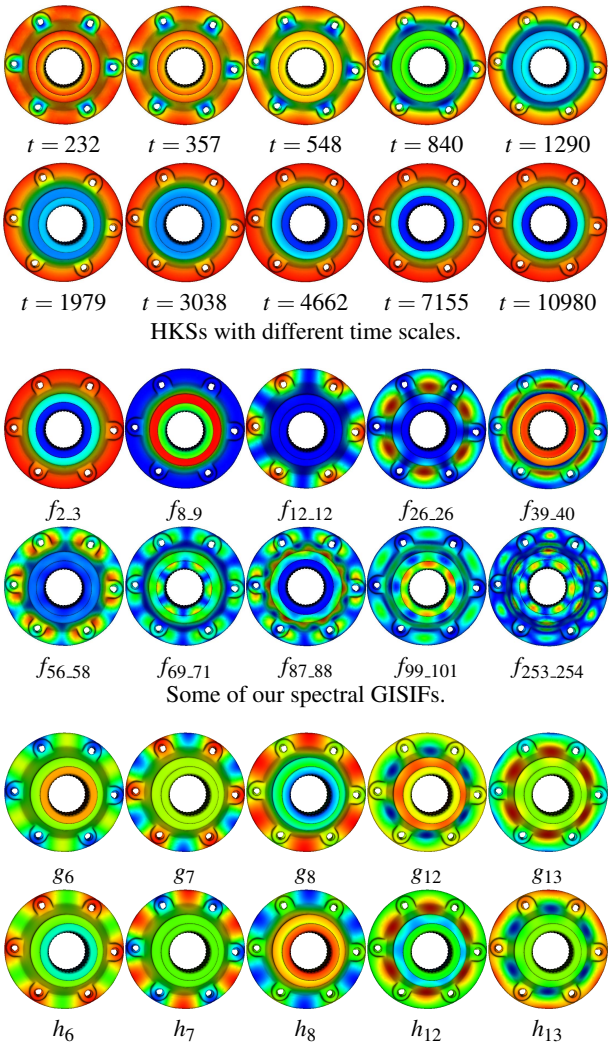

Figure 7: Comparisons of our spectral GISIFs with the HKSs [22]. It can be seen that the HKSs across different time scales (**top**) do not exhibit much variation, while our spectral GISIFs (**center**) and some of their linear combinations (**bottom**) differ significantly from each other, capturing more information.

The HKS and WKS are linear combinations of our spectral GISIFs and so are also GISIFs. In Figure 7, our spectral GISIFs (the center two rows) are compared with with HKSs (the top two rows) across different time scales, where the time scales are the default values in [22]. It can be seen that the HKSs across different time scales do not exhibit much variation, while our spectral GISIFs differ significantly from each other, capturing more information.

Furthermore, for symmetry analysis, our spectral GISIFs are more general (and therefore more flexible) than the symmetry invariant descriptors of HKSs and WKSs. We can use our spectral GISIFs to form other GISIFs rather than HKSs or WKSs. The bottom two rows of Figure 7 show some simple linear combinations of our GISIFs, where g_i, $i \in \{6,7,8,12,13\}$ is the the difference between the GISIF corresponding to the i-th and $(i+1)$-th smallest eigenvalue, and $h_i = -g_i, i \in \{6,7,8,12,13\}$.

Comparisons with the Average Geodesic Distances. Kim et al. pioneered work on GISIFs and propose a class of GISIF based on geodesic distances [6], i.e., Average Geodesic Distances (AGDs) and Minimal Geodesic Distances (MGDs).

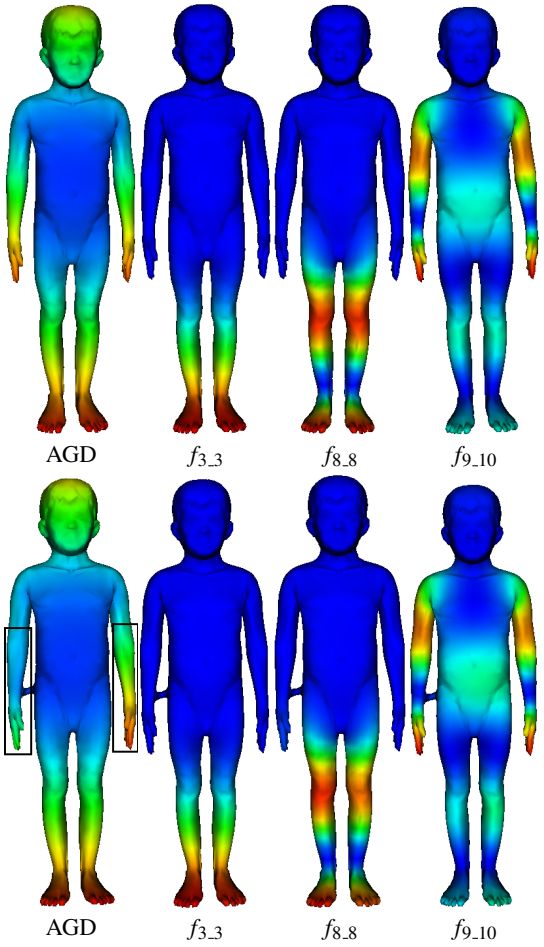

Figure 8: Comparisons between AGDs (**Column 1**) and our spectral GISIFs (**Columns 2, 3, and 4**). **Top:** results on the original mesh. **Bottom:** results on the mesh corrupted by topological noise. Note how the AGD is significantly altered while corresponding GISIFs remain largely unaffected.

In Figure 8, we compare the spectral GISIFs with the AGDs, illustrating that the AGD is sensitive to topological noise while our GISIFs are much more robust. This is due to the fact that small changes in topology, such as the closing of gaps between otherwise geodesically distant limbs, can have a relatively large effect on the AGDs, while the Laplace-Beltrami operator and its corresponding eigenfunctions remain largely unchanged [21].

5 Applications

For a 2D manifold M, in Section 3 we can construct a class of spectral GISIF $f_1, f_2, \ldots, f_n, \ldots$, where f_i corresponds to the i-th smallest eigenvalue (repeated or non-repeated) of the Laplace-Beltrami operator. As in [9], based on these components we can obtain a *Symmetry-Factored Embedding* (SFE) of M as follows

$$\mathrm{SFE}(\mathbf{p}) = (\tilde{f}_1(\mathbf{p}), \tilde{f}_2(\mathbf{p}), \ldots, \tilde{f}_n(\mathbf{p}), \ldots), \tag{9}$$

for $\mathbf{p} \in M$ where $\tilde{f}_i = f_i / \sqrt{\int_M f_i^2(\mathbf{p}) d\mathbf{p}}$ is the normalization of f_i.

The *Symmetry-Factored Distance* (SFD) between points $\mathbf{p}$ and $\mathbf{q}$ on M is defined as the Euclidean distance between their SFEs; i.e.,

$$\mathrm{SFD}(\mathbf{p}, \mathbf{q}) = \sqrt{\sum_{i=1}^{\infty} (\tilde{f}_i(\mathbf{p}) - \tilde{f}_i(\mathbf{q}))^2}. \tag{10}$$

The SFDs between a point and its symmetric points are zero.

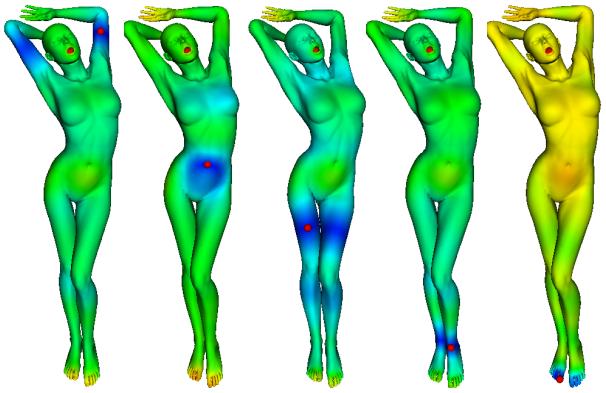

Figure 9: Symmetry-factored distances (SFDs) computed using spectral GISIFs from the red points shown. Note how the SFDs between each point and its symmetric points are near zero (blue).

As stated in Section 4, in practice, we only use the spectral GISIFs corresponding to the first m smallest eigenvalues of the Laplace-Beltrami operator, except for the first eigenvalue whose value is zero and its corresponding GISIF is constant. These selected GISIFs represent the lowest frequency information of the shape. In this paper we use a default value $m = 15$. Figure 9 shows examples of SFDs from different source points, where the SFDs between a point and its symmetric points are close to zero. In the following subsections, we use the above SFEs and SFDs to compute symmetry orbits and symmetry-aware segmentations as in [9].

5.1 Symmetry Orbits

As stated in [9], given a 2D manifold M and its global intrinsic symmetry group $G(M)$, the *Symmetry Orbit* (SO) of a point $\mathbf{p}$ on M is defined as $SO(\mathbf{p}) = \{g(\mathbf{p}) | g \in G(M)\}$. The SFDs from the source point $\mathbf{p}$ form a scalar function on M as follows

$$D_{\mathbf{p}}(\mathbf{q}) = SFD(\mathbf{p},\mathbf{q}) = \sqrt{\sum_{i=1}^{\infty} (\tilde{f}_i(\mathbf{p}) - \tilde{f}_i(\mathbf{q}))^2}, \qquad (11)$$

for $\mathbf{q} \in M$. The function values at the symmetric points of $\mathbf{p}$ are zero, so we can use the points with zero values of the function of Equation (11) to find the symmetry orbit of $\mathbf{p}$. In practice, the function values of Equation (11) on the symmetry orbit of $\mathbf{p}$ are not exactly zero, so we use the local minima of $D_{\mathbf{p}}(\mathbf{q})$ whose function values are close zero to find the symmetry orbit of $\mathbf{p}$. However, the threshold that defines which local minima belong to the symmetry orbit of vertex $\mathbf{p}$ is dependant on the functional values of $D_{\mathbf{p}}(\mathbf{q})$. In practice, it is difficult to give a fixed threshold for all vertices.

Figures 10 and 11 display the symmetry orbits from some source points. The five-point star in Figure 11 has five rotational symmetries and six reflectional symmetries, including the front-back one. The number of points in symmetry orbits of the red points in Figures 11 (a)-(d) are 5, 10, 20 and 20, respectively.

5.2 Symmetry-aware Segmentation

Symmetry is an important cue for segmentation of shapes into functional parts [9, 25]. In this paper, the symmetry-aware segmentation is obtained by performing the standard k-means clustering algorithm on the points in the symmetry-factored embedding space, and then segmenting the input shape based on the resulting clusters. The reason is that the symmetry-factored distance between two points measures how close the two points are to being symmetric, so clusterings of the symmetry-factored embedding in Equation (9) would obtain symmetry-aware segmentations, dividing a point and its symmetric points into the same segment [9].

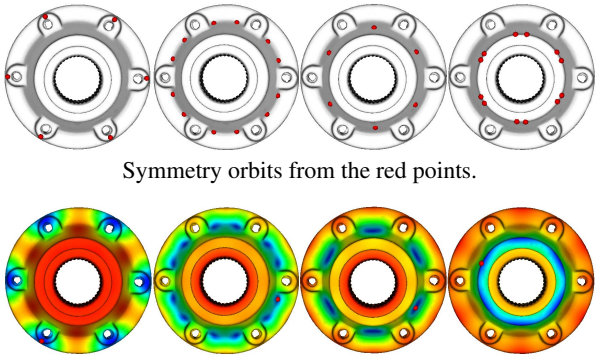

Symmetry orbits from the red points.

Symmetry-factored distances from the same red points.

Figure 10: Symmetry orbits and factored distances computed using spectral GISIFs on a wheel model with rotational symmetries.

Figure 12 shows some results of symmetry-aware segmentation by k-means clustering on the symmetry-factored embedding of a point cloud and triangle mesh with different numbers of clusters without any optimization or postprocessing. It can be seen that each point and its symmetric points are in the same cluster. For example, the cusps of tentacles of the octopus are symmetric, so they are in one segment.

6 Conclusion and Future Work

In this paper, we propose a new class of global intrinsic symmetry invariant functions on compact Riemannnian manifolds, which we call spectral GISIFs, and their discretization onto 2D manifolds approximated either by triangle meshes or point clouds. We've shown spectral GISIFs to be more robust to topological noise than those based on geodesic distances. Furthermore, for symmetry analysis, the proposed spectral GISIFs are more general, flexible, and appear to capture more information than the classical HKSs and WKSs. Generally, our spectral GISIFs, with higher rank than the HKSs and WKSs, have the potential to be useful as symmetry invariant descriptors for shape matching via quotient spaces [14]. As applications, we show how spectral GISIFs can be used to compute symmetry orbits and symmetry-aware segmentations.

There are two main limitations of spectral GISIFs. First, they cannot be computed on non-manifold shapes, a characteristic that is inherited from the Laplace-Beltrami operator not being defined in such cases. Second, it may be difficult for a user to decide which spectral GISIFs to use out of the full available spectrum.

There are several open avenues for future work. First, we would like to investigate automatic methods for choosing the most informative GISIFs, possibly based on entropy. Second, we would like to study the relation between global intrinsic symmetry and the multiplicity of eigenvalues of the Laplace-Beltrami operator. Third, we plan to investigate principled heuristics for automatically setting the threshold ε for deciding whether an eigenvalue is repeated or not. Fourth, while we have shown that the sparsity property holds empirically in the datasets we have worked with, we will investigate if this property is theoretically derivable from the properties of the manifold. Finally, we would like to investigate more applications of spectral GISIFs, including symmetry aware skeletonization, texture synthesis, denoising, repair, and processing and analysis of high-dimensional manifolds.

Acknowledgements

We thank the anonymous reviewers for their valuable comments and suggestions. We are also grateful to Maks Ovsjanikov for sharing the models used in Figure 8. This research is supported in part by the National Natural Science Foundation of China (61173103,

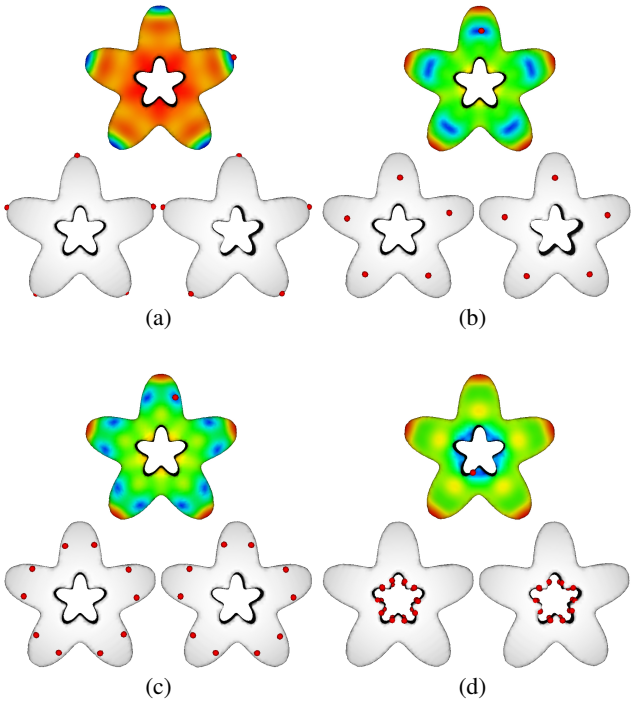

Figure 11: Symmetry factored distances from some points and symmetry orbits of these points on the five-pointed star. In each result, the **top** shows the symmetry factored distance from the red point, and the **bottom** shows the front and back viewpoints of the symmetry orbit of the corresponding red point.

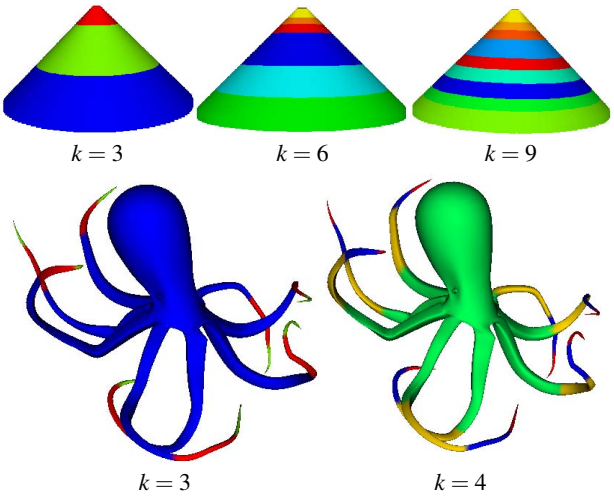

Figure 12: Symmetry-aware segmentations: we use k-means clustering on the SFE of the point cloud of a cone (**top**) and octopus triangle mesh **(bottom).**

F0208), the Natural Sciences and Engineering Research Council of Canada (611370), the Natural Science Foundation of Hebei Province (F2014210127), and Scientific Research Foundation of Shijiazhuang Tiedao University (Z110205).

REFERENCES

[1] M. Aubry, U. Schlickewei, and D. Cremers. The wave kernel signature: a quantum mechanical approach to shape analysis. In *Computer Vision Workshops*, pages 1626–1633, 2011.

[2] M. Belkin, J. Sun, and Y. Wang. Constructing Laplace operator from point clouds in R^d. In *Nineteenth Annual ACM-SIAM Symposium on Discrete Algorithms*, pages 1031–1040, 2009.

[3] M. Chertok and Y. Keller. Spectral symmetry analysis. *IEEE Transactions on Pattern Analysis and Machine Intelligence*, 32(7):1227–1238, 2010.

[4] M. Desbrun, M. Meyer, P. Schröder, and A. H. Barr. Discrete differential-geometry operators for triangulated 2-manifolds. In *Proceedings of Visualization and Mathematics*, pages 35–57, 2002.

[5] K. Gębal, J. A. Bærentzen, H. Aanæs, and R. Larsen. Shape analysis using the auto diffusion function. *Computer Graphics Forum*, 28(5):1405–1413, 2009.

[6] V. G. Kim, Y. Lipman, and X. Chen. Möbius transformations for global intrinsic symmetry analysis. *Computer Graphics Forum*, 29(5):1689–1700, 2010.

[7] B. Lévy. Laplace-Beltrami eigenfunctions: Towards an algorithm that understands geometry. In *Shape Modeling and Applications, invited talk*, 2006.

[8] B. Lévy and H. Zhang. Spectral mesh processing. In *ACM SIGGRAPH Asia Courses*, 2009.

[9] Y. Lipman, X. Chen, I. Daubechies, and T. A. Funkhouser. Symmetry factored embedding and distance. *ACM Transactions on Graphics*, 29(4):439–464, 2010.

[10] C. Luo, I. Safa, and Y. Wang. Approximating gradients for meshes and point clouds via diffusion metric. *Computer Graphics Forum*, 28(5):1497–1508, 2009.

[11] N. J. Mitra, L. J. Guibas, and M. Pauly. Partial and approximate symmetry detection for 3D geometry. *ACM Transactions on Graphics*, 25(3):560–568, 2006.

[12] N. J. Mitra, M. Pauly, M. Wand, and D. Ceylan. Symmetry in 3D geometry: extraction and applications. *Computer Graphics Forum*, 32(6):1–23, 2013.

[13] M. Ovsjanikov, Q. Mérigot, F. Mémoli, and L. J. Guibas. One point isometric matching with the heat kernel. *Computer Graphics Forum*, 29(5):1555–1564, 2010.

[14] M. Ovsjanikov, Q. Mérigot, V. Pătrăucean, and L. Guibas. Shape matching via quotient spaces. *Computer Graphics Forum*, 32(5):1–11, 2013.

[15] M. Ovsjanikov, J. Sun, and L. Guibas. Global intrinsic symmetries of shapes. *Computer Graphics Forum*, 27(5):1341–1348, 2008.

[16] M. Ovsjanikovs. *Spectral methods for isometric shape matching and symmetry detection*. PhD thesis, Stanford University, Stanford, 2011.

[17] U. Pinkall and K. Polthier. Computing discrete minimal surfaces and their conjugates. *Experimental Mathematics*, 2(1):15–36, 1993.

[18] D. Raviv, A. M. Bronstein, M. M. Bronstein, and R. Kimmel. Symmetries of non-rigid shapes. In *International Conference on Computer Vision*, pages 1–7, 2007.

[19] M. Reuter, F.-E. Wolter, and N. Peinecke. Laplace-Beltrami spectra as a shape-DNA of surfaces and solids. *Computer-Aided Design*, 38(4):342–366, 2006.

[20] S. Rosenberg. *The Laplacian on a Riemannian Manifold*. Cambridge University Press, 1997.

[21] R. M. Rustamov. Laplace-Beltrami eigenfunctions for deformation invariant shape representation. In *Eurographics Symposium on Geometry Processing*, pages 225–233, 2007.

[22] J. Sun, M. Ovsjanikov, and L. J. Guibas. A concise and provably informative multi-scale signature sased on heat diffusion. *Computer Graphics Forum*, 28(5):1285–1295, 2009.

[23] B. Vallet and B. Lévy. Spectral geometry processing with manifold harmonics. *Computer Graphics Forum*, 27(2):251–260, 2008.

[24] M. Wardetzky, S. Mathur, F. Kälberer, and E. Grinspun. Discrete Laplace operators: No free lunch. In *Eurographics Symposium on Geometry Processing*, pages 33–37, 2007.

[25] K. Xu, H. Zhang, W. Jiang, R. Dyer, Z. Cheng, L. Liu, and B. Chen. Multi-scale partial intrinsic symmetry detection. *ACM Transactions on Graphics*, 31(6), 2012.

[26] X. G. Yang Liu, Balakrishnan Prabhakaran. Point-based manifold harmonics. *IEEE Transactions on Visualization and Computer Graphics*, 18(10):1696–1703, 2012.